Available online at www.sciencedirect.com
SCIENCE DIRECT®

Journal of the European Ceramic Society 23 (2003) 2143–2152
www.elsevier.com/locate/jeurceramsoc

Microstructure development and dielectric properties of hydrothermal $BaTiO_3$ thin films

Mark A. McCormick[1], Elliott B. Slamovich*

School of Materials Engineering, Purdue University, West Lafayette, IN 47907-1289, USA

Received 10 June 2002; received in revised form 2 December 2002; accepted 15 December 2002

Abstract

Polycrystalline $BaTiO_3$ thin films were processed hydrothermally by reacting TiO_2 films at 90 °C in alkaline solutions containing Ba^{2+}. Films grown on (100) $SrTiO_3$ suggested that $BaTiO_3$ nucleation occurred at the film-substrate interface as well as the film-solution interface. As-reacted $BaTiO_3$ films grown on Pt-coated glass substrates had a dielectric constant and tanδ of 80 and 0.20 respectively. Current–voltage (*I–V*) measurements suggested that the leakage mechanism combined aspects of Poole–Frenkel and Schottky-barrier controlled processes, and had an associated metal/ceramic barrier height of 0.46 eV. Annealing the $BaTiO_3$ films at 200–500 °C in air resulted in lower values for dielectric constant, tanδ, and leakage current, and a larger barrier height.

Keywords: $BaTiO_3$ and titanates; Capacitors; Dielectric properties; Films; Hydrothermal methods

1. Introduction

A high dielectric constant, low leakage current, and high dielectric breakdown strength are characteristic of perovskite materials such as $BaTiO_3$. These properties make $BaTiO_3$ thin films attractive for a variety of applications, including microwave devices, dynamic random access memories (DRAMs), and multilayer capacitors.[1–5] For example, using a high dielectric constant material like $BaTiO_3$ as a capacitor material allows more charge storage per unit area, facilitating fabrication of smaller devices. Furthermore, the large polarizability and low leakage current typical of $BaTiO_3$ films make them suitable for thin film capacitors in applications such as high-density DRAM.

Processing routes to $BaTiO_3$, including sputtering, MOCVD, laser ablation, and sol-gel processing generally require deposition temperatures or heat treatments in excess of 500 °C.[5–9] At these temperatures, undesirable interdiffusion between thin films, contact electrodes, and substrates may occur. Furthermore, thermal stresses developed during cooling may cause cracking and/or affect the long-term reliability of the device.[10,11] To help alleviate these concerns, hydrothermal processing, a low-temperature route (< 100 °C) to synthesize crystalline ceramics in an aqueous medium, may be used. The hydrothermal medium is attractive for thin film synthesis because the desirable product can be stabilized by manipulation of chemical process variables such as solution pH, temperature, and pressure, while inhibiting undesirable compound formation.[12] Furthermore, hydrothermal synthesis is a simple and low-cost method for preparing $BaTiO_3$ films from a variety of precursor materials. The product is generally highly pure, stoichiometric, homogenous, and composed of fine-grain crystals with a narrow size distribution.[13]

This paper examines the microstructure evolution and dielectric properties of hydrothermally derived $BaTiO_3$ thin films. Microstructure evolution is examined by growing films on (100) $SrTiO_3$ single crystal substrates, while dielectric properties are evaluated by growing films on Pt-coated glass substrates. Dielectric properties including the dielectric constant, tanδ, and leakage current are characterized in both as-reacted and annealed films. Finally, leakage current measurements as a function of applied field, temperature, and electrode material are used to assess the conduction mechanisms active in the thin films.

* Corresponding author.
E-mail address: elliotts@ecn.purdue.edu (E.B. Slamovich).
[1] Present address: Intel Corporation, Portland, OR, USA.

0955-2219/03/$ - see front matter © 2003 Elsevier Science Ltd. All rights reserved.
doi:10.1016/S0955-2219(03)00022-0

2. Experimental

$BaTiO_3$ thin films were processed by spin-casting. Titanium dimethoxy dineodecanoate (TDD), synthesized by the method of Xu et al., was used as the Ti source.[14] TDD was chosen for the precursor film because of a high resistance to cracking during drying relative to other Ti metal–organic precursors.[15–17] TDD was diluted with p-xylene to a viscosity of approximately $5{\cdot}10^{-3}$ Pa s resulting in films 0.4–0.5 μm thick after spin-casting onto Pt-coated glass substrates at 8000 rpm for 20 s. Pt was chosen for the electrode material for its large work function, which creates a large potential barrier between the film and the electrode, thereby minimizing capacitor leakage during electrical property measurements.[18] The TDD was pyrolyzed in air at 400 °C to form a dense layer of TiO_2, a requirement to process dense $BaTiO_3$ films.[19] A second TDD layer 0.4–0.5 μm thick was applied and pyrolyzed. Layering prevented precursor cracking during firing, while providing sufficient Ti for conversion to a continuous $BaTiO_3$ film. The final thickness of the bi-layer precursor film was approximately 0.2 μm, as determined by surface profilometry and cross-section scanning electron microscopy (SEM) (JSM-3 5CF, Jeol Ltd.). Aqueous solutions of $Ba(OH)_2$ were prepared by boiling deionized water to remove dissolved CO_2, and adding the appropriate amount of $Ba(OH)_2{\cdot}8H_2O$ to produce solutions within the concentration range of 0.5–1.0 M. The water of hydration of the Ba^{2+} source was taken into account when calculating the volume of water and mass of hydroxide required for the desired molarity. The precursor films were placed into a 35 ml polyethylene bottle containing aqueous $Ba(OH)_2$, sealed, and placed into a preheated forced-air oven to react at 90 °C for up to 24 h. After reaction, films were removed from the $Ba(OH)_2$ solution in a nitrogen atmosphere to avoid formation of $BaCO_3$ on the $BaTiO_3$ film surface, rinsed with a warm aqueous ammonium hydroxide solution (pH > 12), and then rinsed again in warm ethanol to facilitate drying. $BaTiO_3$ films were fabricated on (100) oriented $SrTiO_3$ substrates using a similar procedure, except that a Pt coating was not deposited on the substrate, and the films were reacted in 2.0 M $Ba(OH)_2$ at 90 °C for 4 h.

Wavelength dispersive spectroscopy (WDS) (SX-50, Cameca Instruments Co.) was used to confirm complete conversion of TiO_2 to $BaTiO_3$. Film crystallinity was examined using X-ray diffraction (XRD) (D500, Siemens Analytical X-Ray Instruments Inc.), scanning over 20–35° 2θ at 1.2°/min, using Cu K_α radiation ($\lambda = 1.54$ Å). Lattice parameters were determined from the (110) peak, fitting the data using a split Pearson VII function.[20] To ensure the accuracy of peak positions extracted from the XRD data, a film of Ag was deposited by evaporation onto a small portion of the $BaTiO_3$ film surface for use as an internal standard. The change in the $BaTiO_3$ lattice parameter was examined as a function of post-deposition annealing for temperatures up to 500 °C. Atomic force microscopy (AFM) was used to measure thin film roughness, and film grain size was measured using the line intercept method.

Planar capacitors were assembled using photolithography to sputter circular Pt electrodes 110 μm in diameter onto the film surface. Capacitance and dielectric loss (tanδ) measurements were performed at room temperature using a LCR meter (HP 4275A) at 10 kHz–10 MHz with an applied potential of 0.10 V. After recording the dielectric properties for the as-formed films, they were heated to 150 °C for 30 min in air, and the DC leakage current as a function of applied voltage (I–V) was measured as a function of temperature over the range 25–150 °C to determine the conduction barrier height. The I–V measurement was performed using a Keithley 238 Source-Measurement Unit to apply a staircase series of voltage steps as described by Dietz and Waser, and to measure the resulting current across the capacitor.[21] DC voltages over the range −15 to +15 V (corresponding to fields of approximately ±315 kV/cm), with a step size of 1.0 V, were used. The leakage current was measured 1.0 s after applying the voltage to account for polarization currents. Films were annealed in either flowing O_2 or Ar–5% H_2 (i.e. oxidizing or reducing atmospheres) at 500 °C, and the I–V properties were re-evaluated to examine the effect of annealing on the leakage behavior and barrier height. Varying combinations of materials for the top and bottom electrodes (Pt, Au, Ag) were used to help determine the conduction mechanism.

3. Results and discussion

3.1. Reaction kinetics and microstructural development

The time required for complete conversion of TiO_2 precursor films to $BaTiO_3$ was determined using WDS to examine the Ba:Ti ratio, where a 1:1 Ba:Ti ratio indicated complete conversion. Films reacted at 90 °C in 0.5 M $Ba(OH)_2$ required approximately 24 h to form a film with a 1:1 ratio of Ba:Ti (Fig. 1). The error bars in Fig. 1 represent the scatter in data from five points on the film sampled at random. Peaks corresponding to TiO_2 were absent from the XRD patterns from films processed for more than 4 h, suggesting that films with a 1:1 Ba:Ti ratio were phase-pure $BaTiO_3$. The reaction rate increased dramatically in 1.0 M $Ba(OH)_2$, requiring 1–2 h for complete conversion from TiO_2 to $BaTiO_3$.

Thin film deposition directly onto single crystal (100) $SrTiO_3$ substrates (with no Pt layer) was used to examine film nucleation and growth behavior. In a randomly oriented $BaTiO_3$ sample, the (110) reflection has the

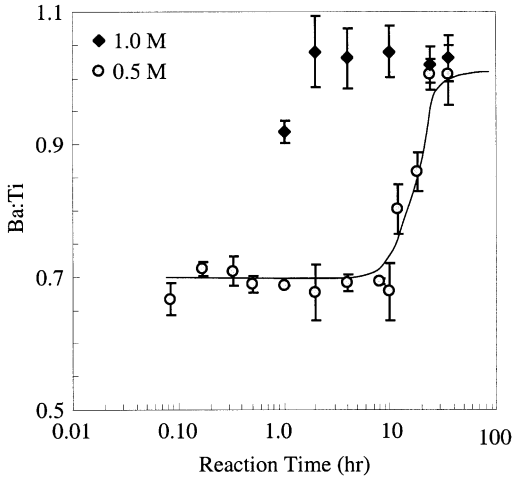

Fig. 1. WDS data of the Ba:Ti ratio for $BaTiO_3$ thin films processed at 90 °C in 1.0 M (◆) and 0.5 M (○) $Ba(OH)_2$.

greatest intensity, while the (100) and (111) reflections have intensities 14% and 30% of the (110) reflection respectively.[22] XRD data suggests that the $BaTiO_3$ films grown on (100) $SrTiO_3$ substrates were textured (Fig. 2a), with preferential orientation corresponding to the substrate orientation. The degree of texture was quantified by comparing the relative integrated peak intensities of the (100), (110), and (111) reflections to a random sample, based on the JCPDS peak intensity values for cubic $BaTiO_3$.[22] The multiples of a random distribution (MRD) for each of these reflections was calculated using:

Table 1
MRD values for $BaTiO_3$ thin films

Peak index	$BaTiO_3$ on $SrTiO_3$ MRD	$BaTiO_3$/Pt/glass MRD
(100)	4.4	1.7
(110)	0.6	1.0
(111)	0.7	0.6

$$\mathrm{MRD} = \frac{\left(\dfrac{I_{hkl}(o)}{I_{100}(o)+I_{110}(o)+I_{111}(o)}\right)}{\left(\dfrac{I_{hkl}(r)}{I_{100}(r)+I_{110}(r)+I_{111}(r)}\right)} \quad (1)$$

where $I_{hkl}(o)$ is the integrated peak intensity of the (*hkl*) peak for the oriented thin film, and $I_{hkl}(r)$ is the relative peak intensity for the JCPDS standard. This calculation was also performed for a nominally random $BaTiO_3$ film deposited on a Pt-coated glass substrate (Fig. 2b). The results are summarized in Table 1. A MRD value of 1.7 was obtained for the (100) reflection in the nominally random $BaTiO_3$ film, while the $BaTiO_3$ film grown on (100) $SrTiO_3$ had a MRD value of 4.4 indicating a strong (100) preferred orientation.

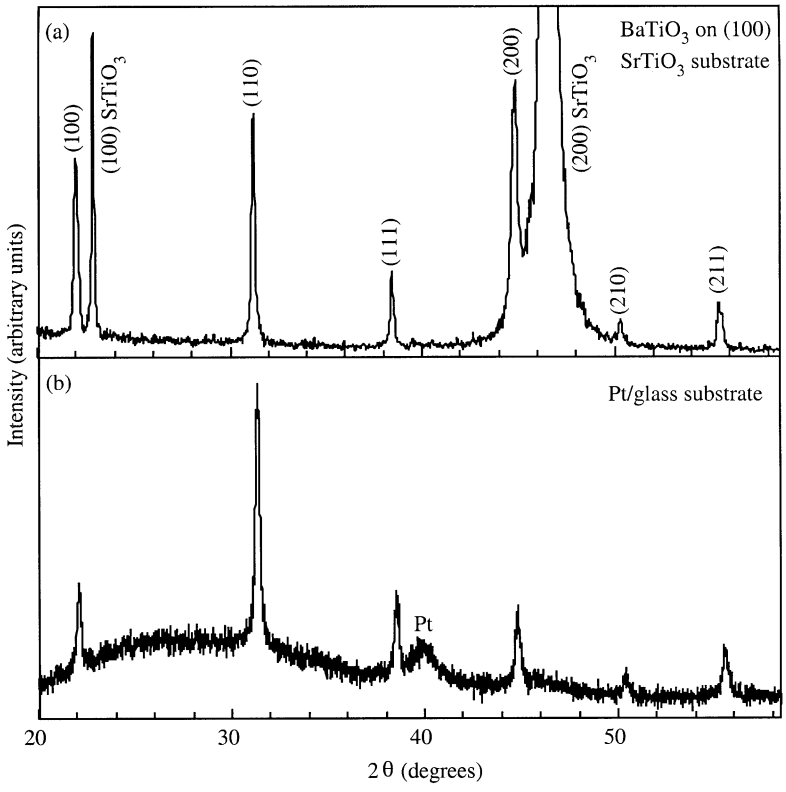

Fig. 2. XRD spectra for $BaTiO_3$ thin films deposited (a) directly on single crystal <100> $SrTiO_3$ and (b) on a Pt-coated glass substrate. Both films were reacted at 90 °C in 2.0 M $Ba(OH)_2$ for 4 h.

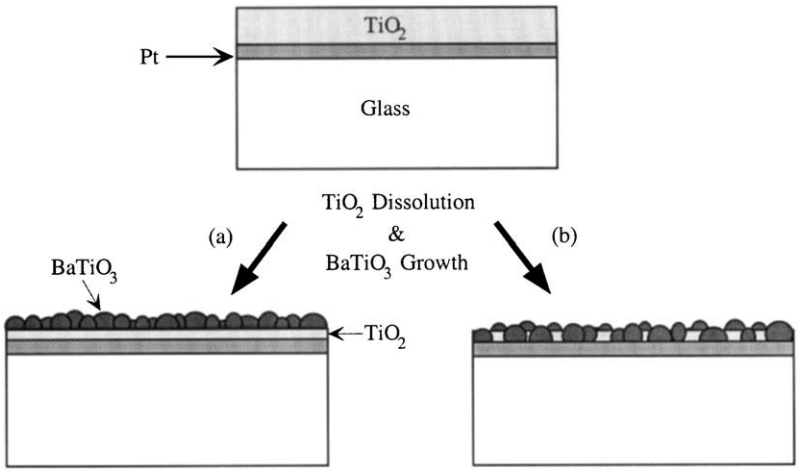

Fig. 3. Schematic illustration $BaTiO_3$ film growth from the TiO_2 precursor layer. (a) growth occurring exclusively at the film–solution interface, and (b) growth occurring at both film–solution and film–substrate interfaces.

At least two possible scenarios for $BaTiO_3$ film growth may be visualized. First, the exposed TiO_2 surface dissolves, and heterogeneous nucleation of $BaTiO_3$ occurs at the film/solution interface (Fig. 3a). Second, diffusion of Ba^{2+} through the TiO_2 film results in heterogeneous nucleation of $BaTiO_3$ at the film/substrate interface (Fig. 3b). The first scenario favors the formation of a layered structure as the conversion reaction proceeds to completion, while the second scenario favors a mixture of phases in which isolated islands of TiO_2 remain between growing $BaTiO_3$ particles.

Textured $BaTiO_3$ film growth indicates that particle nucleation occurred at least in part at the film/substrate interface (Fig. 3b). Examining the dielectric constant of the $BaTiO_3/TiO_2$ composite films from Fig. 1 processed in 0.5 M $Ba(OH)_2$ provides further evidence of a structure with isolated TiO_2 islands prior to complete conversion to $BaTiO_3$. The dielectric properties of these films exhibited little dependence on the amount of residual TiO_2 after approximately 70% conversion to $BaTiO_3$ (Fig. 4). The simplest case for mixtures of ideal dielectrics can be considered on the basis of two layers of material with different dielectric constants either normal or parallel to the capacitor plates. When the layers are normal to the plates, the capacitance is additive; when they are parallel, the *inverse* capacitance is additive (i.e. $1/C = v_1/C_1 + v_2/C_2$, where v_i = volume fraction). Thus, for normal layers, the effective dielectric constant of the composite increases linearly as a high κ' phase is added to a low κ' phase. For parallel layers, the dielectric constant remains relatively low until the low κ' layers are very thin (i.e. $\leqslant 10$ vol%).[23] The small variation in the dielectric constant for $BaTiO_3/TiO_2$ composite films in this study provides evidence against a layered structure formed by a reaction front (Fig. 3a). The isolated TiO_2 island structure would minimize the effect of residual TiO_2 on the dielectric constant, reflecting the behavior shown in Fig. 4.

The remainder of this manuscript will focus on $BaTiO_3$ films processed on Pt-coated glass substrates in 1.0 M $Ba(OH)_2$ for 4 h at 90 °C. These processing conditions resulted in films with a typical average grain size of approximately 75 nm and a RMS surface roughness of approximately 8 nm as measured by the line intercept method, and AFM respectively. XRD patterns of these films were similar to the pattern shown in Fig. 2b indicating that the films had a cubic crystal structure. While the tetragonal polymorph is the stable form of $BaTiO_3$ at room temperature, it is common to observe the metastable cubic polymorph in $BaTiO_3$ films and powders processed hydrothermally.[24–26] Further, the

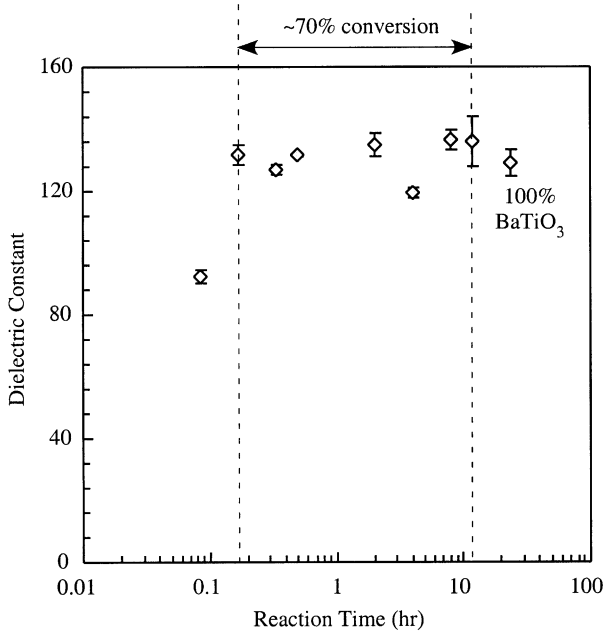

Fig. 4. Dielectric constant as a function of reaction time for $BaTiO_3$ thin films processed at 90 °C in 0.5 M $Ba(OH)_2$. The error bars represent the scatter in data collected from five capacitors sampled at random across the film surface.

JCPDS standard for cubic $BaTiO_3$ is prepared by the hydrolysis of a titanium alkoxide in an aqueous solution of barium hydroxide. In the JCPDS standard, the tetragonal polymorph is observed after heating to 800 °C and cooling to room temperature.[22]

3.2. $BaTiO_3$ lattice parameter

As processed, $BaTiO_3$ films reacted in 1.0 M $Ba(OH)_2$ for 4 h at 90 °C had a lattice parameter of 4.04 Å, somewhat larger than the JCPDS value of 4.03 Å for cubic $BaTiO_3$, and significantly larger than the 3.99 Å value cited for the a-axis in tetragonal $BaTiO_3$.[25,27] Annealing the films for 30 min in air resulted in a marked decrease in the film lattice parameter at 200 °C, and a decrease in the unit cell volume of over 1% from the as-formed film after annealing at 500 °C (Fig. 5).

Several studies suggest that chemically bound hydroxyl (OH^-) groups are incorporated directly into the perovskite lattice, presumably on oxygen sites.[25,28–31] Infrared spectroscopy (IR) indicated that heat treatments up to 600 °C resulted in a marked decrease in lattice hydroxyl group incorporation, accompanied by a decrease in the unit cell volume.[25,28–31] Wada et al. concluded that lattice expansion in hydrothermally derived $BaTiO_3$ films is due a reduction in ionic bonding strength resulting from lattice defects such as hydroxyl groups and charge-compensating vacancies.[30] Furthermore, they suggested that there are two kinds of hydroxyl groups in hydrothermal $BaTiO_3$ particles: surface-adsorbed OH^- and lattice OH^-. They stated that surface-adsorbed groups have a range of bonding energies, because their adsorption may vary in coordination number, while lattice hydroxyl groups have only a specific bonding energy in the $BaTiO_3$ lattice. They used a combination of IR data and differential thermal analysis with thermogravimetry to quantify hydroxyl group desorption as a function of temperature.[28,30] Their results suggest that surface hydroxyl desorption occurs from room temperature to 600 °C, and lattice hydroxyl groups are released over the narrow temperature range of 300–400 °C.

Since it seems unlikely that desorption of surface hydroxyl groups would significantly effect the lattice parameter, the decrease in lattice parameter documented in Fig. 5 suggests that lattice hydroxyl desorption occurs at temperatures below 200 °C, and continues until at least 500 °C.

3.3. Dielectric properties

3.3.1. Dielectric constant and dielectric loss

Typical values of the dielectric constant and dielectric loss (tanδ) for $BaTiO_3$ films reacted in 1.0 M $Ba(OH)_2$ at 90 °C for 4 h were 82 and 0.25 respectively. Annealing hydrothermal $BaTiO_3$ films at 300 °C for 30 min in air resulted in decreases in both the dielectric constant, to 38, and tanδ, to 0.045 (Fig. 6). The largest change in the dielectric constant and tanδ occurred during annealing between 100 and 200 °C, and slowed considerably with increasing temperature. Chien et al. reported similar results for epitaxial hydrothermal $BaTiO_3$ thin films, where the dielectric constant and tanδ of the as-synthesized films decreased from 450 to 200 and 1.0 to 0.08, respectively, following heating to 300 °C.[29] Fig. 7 shows the dielectric constant and dielectric loss as a function of frequency over the range of 10 kHz–10 MHz for a film reacted in 1.0 M $Ba(OH)_2$ at 90 °C for 4 h, and following annealing at 300 °C in air for 30 min. In the as-formed condition, where hydroxyl defects were abundant, the polarizability and loss were both strongly frequency dependent. However, annealing at 300 °C resulted in a dielectric constant that was independent of frequency over the measured range.

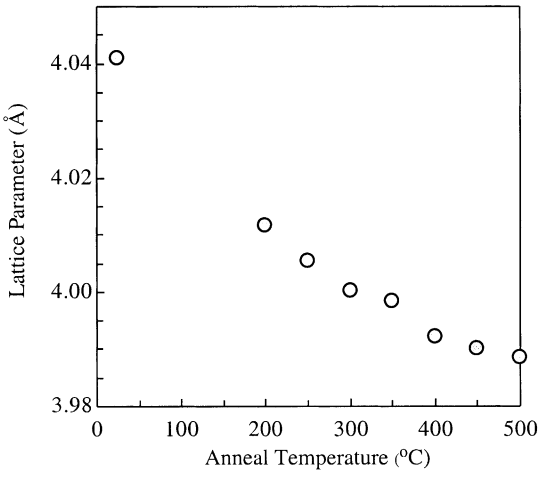

Fig. 5. Change in $BaTiO_3$ lattice parameter following a 30 min anneal in air for a $BaTiO_3$ thin film processed in 1.0 M $Ba(OH)_2$ at 90 °C for 4 h.

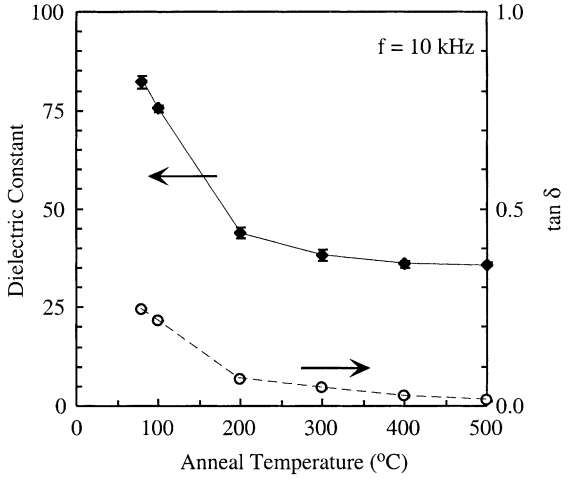

Fig. 6. Dielectric constant (◆) and dielectric loss (○) at 10 kHz as a function of annealing temperature for a $BaTiO_3$ thin film processed in 1.0 M $Ba(OH)_2$ at 90 °C for 4 h.

At first glance, the larger dielectric constant in the as-formed films could be attributed to an increased polarizability associated with an expanded unit cell due to adsorbed hydroxyl groups. However, the magnitude of the decrease in the dielectric constant and tanδ, along with the change in frequency dependence of these properties, suggests that the hydroxyl groups provide their own contribution to $BaTiO_3$ polarizability. For example, the higher dielectric constant and tanδ of the as-formed films could be attributed to the reconfiguration of lattice and surface adsorbed hydroxyl groups in response to the alternating electric field. When an ac field is applied at sufficiently low frequencies (e.g. 10 kHz), the hydrogen and oxygen ions can exchange positions. This switchable dipole contributes to the net polarization (or capacitance), and the time lag with the applied ac field contributes to dielectric loss. Annealing of hydrothermal films in air leads to hydroxyl group desorption in the form of water, where two hydroxyl defects are replaced by a single oxygen vacancy.[25] The same mechanism is a plausible explanation for the observed change in frequency dependence of the dielectric constant and tanδ. Low-frequency polarization effects are typically due to dipole rotations between equivalent positions within the lattice. In this case, the motion of hydroxyl defects may provide this type of polarization. Elimination of hydroxyl defects upon annealing eliminates this low-frequency dipole contribution to the polarizability. Furthermore, the gradual reduction in polarization for the as-formed films over the frequency range 10 kHz–10 MHz, as opposed to a sharp drop-off at a specific frequency, indicates that not all hydroxyl defects in $BaTiO_3$ are equivalent, and therefore resonate at different frequencies. For example, surface-adsorbed hydroxyl groups would likely resonate at different frequencies than lattice-bound hydroxyl ions, or hydroxyl ions residing at grain boundaries.

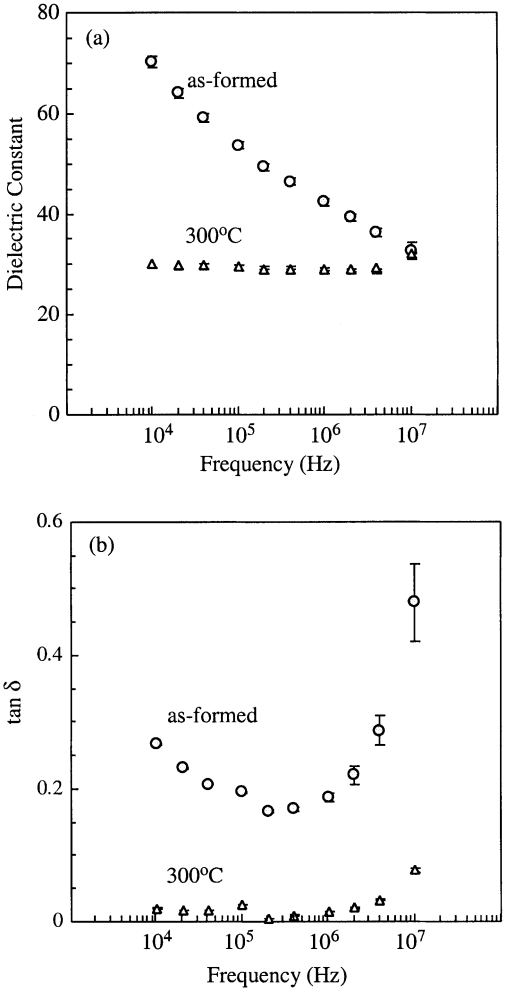

Fig. 7. (a) Dielectric constant and (b) dielectric loss as a function of frequency for $BaTiO_3$ films processed in 1.0 M $Ba(OH)_2$ at 90 °C for 4 h, and following annealing at 300 °C in air for 30 min.

The dielectric constant and dielectric loss of a $BaTiO_3$ film processed in 1.0 M $Ba(OH)_2$ at 90 °C for 4 h was also examined following annealing at 500 °C in either pure oxygen or a Ar–5% H_2 atmosphere. The results, summarized in Table 2, show that the dielectric constant and tanδ exhibited little dependence on the pO_2 of the annealing atmosphere. This indicates that the higher dielectric constant and dielectric loss in the as-formed films was primarily due to the presence of hydroxyl defects, and that variations in the concentration of oxygen vacancies due to different annealing atmospheres was at most a second order effect.

3.4. Current–voltage characterization

Interpretation of the relationship between leakage current density and applied electric field (I–V curves) for $BaTiO_3$ thin films must be done with care, since slow polarization currents can prevent observation of the true leakage behavior. Therefore, a voltage step measurement approach described by Dietz et al.[21] was used to separate the polarization and leakage currents. Fig. 8 shows I–V data for a $BaTiO_3$ thin film processed at 90 °C for 4 h in 1.0 M $Ba(OH)_2$, and following annealing at 500 °C in either flowing O_2 or Ar–5% H_2. The data shown is for a single film, but it represents the behavior observed in several films processed using the same conditions. The data is plotted on a log scale to amplify the transition in conduction from ohmic, below approximately 100 kV/cm, to conduction limited by

Table 2
Dielectric constant and dielectric loss for a $BaTiO_3$ thin film

	Dielectic constant	Dielectic loss
As-formed	100	0.24
O_2 anneal	45	0.026
Ar–5% H_2 anneal	42	0.015

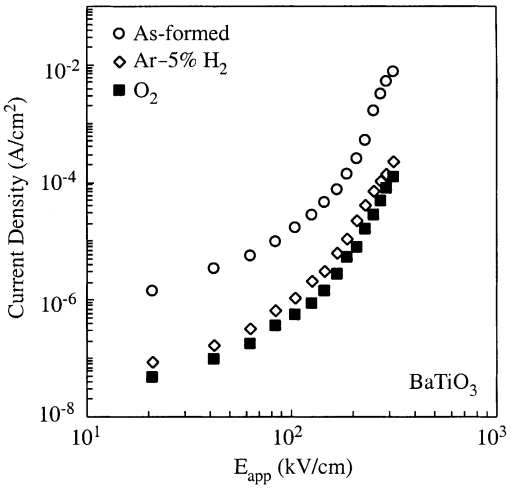

Fig. 8. Leakage current as function of applied electric field for a $BaTiO_3$ film processed in 1.0 M $Ba(OH)_2$ at 90 °C for 4 h, and following annealing for 30 min at 500 °C in flowing Ar–5% H_2 or O_2.

thermionic emission of electrons at higher fields.[21,32] The leakage current for both annealed films was more than an order of magnitude lower than that of the as-formed films, and the effects of the O_2 and Ar–5% H_2 anneals differed only slightly. This suggests that the reduction in leakage was due principally to the elimination of hydroxyl defects and/or interface states, which occurred regardless of annealing atmosphere. However, oxygen vacancies may also play a role in the conduction behavior, perhaps by the introduction of trapping centers into the band gap that tend to increase leakage.

The leakage current mechanisms commonly reported in dielectric thin films include ohmic conduction (usually at low fields), space-charge-limited conduction (SCLC), Poole–Frenkel conduction, and Schottky conduction.[33] Space-charge-limited conduction occurs when electrons are easily injected from the contact into the conduction band of the insulator, and the injected electrons form a space charge layer that limits current flow. For systems in which SCLC is the dominant conduction mechanism, ohmic contacts or contacts with a similar low resistance (i.e. low barrier height for easy thermionic emission) are required for appreciable current flow. Therefore, SCLC is unlikely for the Pt/$BaTiO_3$ system at moderate to high electric fields.[34] Poole–Frenkel conduction occurs when carriers are emitted from trapping centers in the bulk of the film. Conduction is associated with the field-enhanced thermal excitation of charge carriers from these traps, and is sometimes referred to as the 'internal Schottky effect.' Schottky conduction occurs via field-dependent thermal emission from the electrode into the conduction band of the dielectric over a potential barrier. Similar to Poole–Frenkel conduction, the *effective* barrier height is dependent on the magnitude of the applied electric field.

Experimental results reported by McCormick et al.[32] suggested that Schottky-barrier limited conduction was the dominant leakage mechanism in hydrothermally-derived $Ba_xSr_{1-x}TiO_3$ thin films for applied fields >100 kV/cm. A barrier height of 0.56 eV was reported, which is significantly lower than the ideal value of 2.9 eV, based on the difference between the Pt work function ($\Phi_B = 5.4$ eV) and the electron affinity of $BaTiO_3$ ($\chi = 2.5$ eV).[35,36] It was suggested that this discrepancy may be due to a high density of interface states, and annealing may increase the barrier height. However, the role of trapping centers may have been overlooked in this study. Hydrothermally-derived $BaTiO_3$ thin films are known to have a very high concentration of inherent defects.[37] Jonscher and Hill point out that conduction mechanisms in insulating films are intrinsically related to the density of charged defects.[38] If a film contains a high density of positively charged traps, a Poole–Frenkel mechanism should dominate; otherwise a Schottky-barrier limited conduction mechanism is possible. Considering this, if annealing changes the defect and electron concentrations, trapping centers in the bulk of the film may play a role in the conduction behavior. For this reason, both Schottky conduction and Poole–Frenkel conduction were investigated as potential leakage mechanisms.

Leakage current was measured as a function of applied field at room temperature, and as a function of temperature up to 150 °C for $E_{app} = 315$ kV/cm. Films were heated to 150 °C in air for 30 min and cooled to room temperature prior to taking measurements. A linear fit was obtained for the relation ln(J) vs. $\sqrt{E}$ for a $BaTiO_3$ film reacted in 1.0 M $Ba(OH)_2$ at 90 °C for 4 h, shown in Fig. 9 in the as-formed condition, and following O_2 or Ar–5% H_2 anneals at 500 °C for 30 min. This indicates that conduction is controlled by either a Schottky process or a Poole–Frenkel process, where

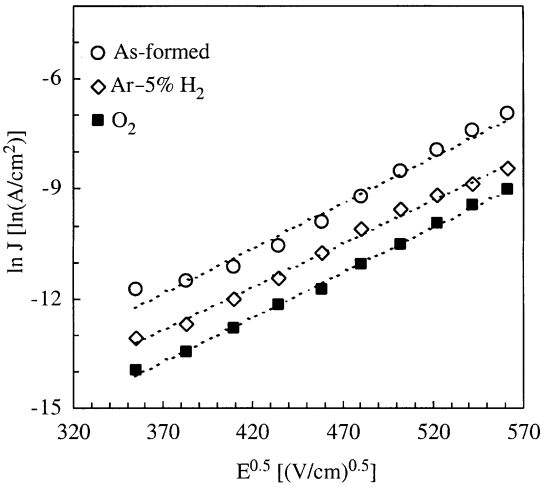

Fig. 9. Schottky plot for a $BaTiO_3$ film processed in 1.0 M $Ba(OH)_2$ at 90 °C for 4 h, following heating to 150 °C in air, and after annealing for 30 min at 500 °C in flowing Ar–5% H_2 or O_2.

field-dependent lowering of the energy barrier causes an increase in conduction with the applied field. The temperature and field dependence of Schottky-controlled leakage current is given by:[33,39]

$$J = A^{**}T^2\exp\left(aE^{1/2} - W_B/k_bT\right) \quad (2)$$

where A^{**} is the effective Richardson constant (which incorporates carrier mobility), a another constant, E is the applied electric field, W_B is the zero-field barrier height, k_b is the Boltzmann constant, and T is temperature. By comparison, the leakage current according to the Poole–Frenkel conduction mechanism is given by:[33,39]

$$J = A_oE\exp\left(\beta E^{1/2} - Q/k_bT\right) \quad (3)$$

where A_o and β are constants, and Q is the depth of the trap potential well. These mechanisms exhibit a qualitatively similar dependence on the applied field. One method of discerning the dominant leakage current mechanism is through the temperature dependence of the leakage, as shown in Fig. 10. If conduction is dominated by thermionic emission at the electrode-ceramic interface, a plot of $\ln(J/T^2)$ vs. $1/T$ yields a straight line (Fig. 10a); if Poole–Frenkel conduction dominates, a plot of $\ln(J/E)$ vs. $1/T$ provides a linear fit (Fig. 10b). The barrier height (W_B), or trap depth (Q) is then extracted from either the slopes or intercepts of the temperature and field dependent plots.[21,40] The Schottky plot for the films in this study under positive applied fields yielded a linear response. However, an equally good linear fit was obtained for the same data when plotted as $\ln(J/E)$ vs. $1/T$. The barrier heights and trap depths, calculated using Eqs. (2) and (3) and the data in Fig. 10, are summarized in Table 3. While annealing raised the barrier height, these values still deviate significantly from ideal.

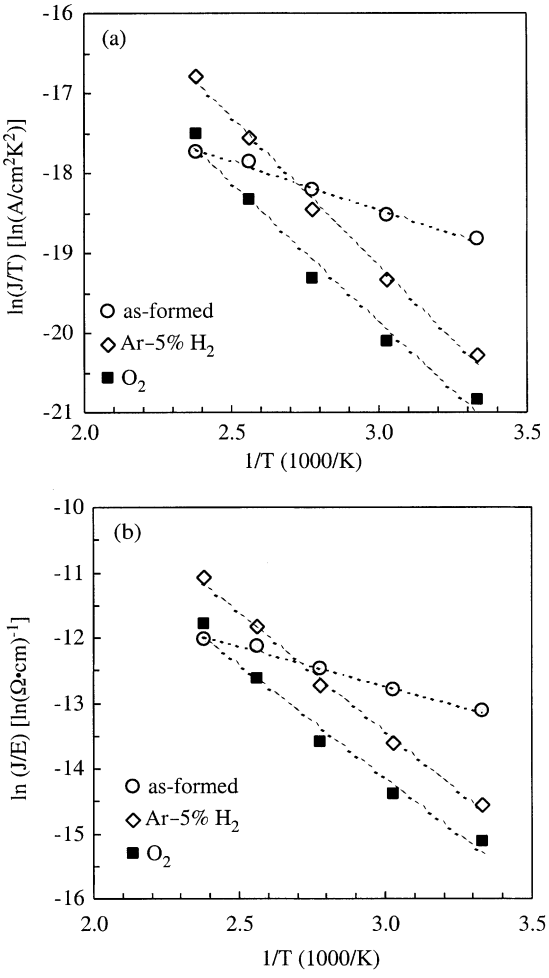

Fig. 10. (a) Schottky plot and (b) Poole–Frenkel plot for a $BaTiO_3$ film processed in 1.0 M $Ba(OH)_2$ at 90 °C for 4 h, and following annealing for 30 min at 500 °C in flowing Ar–5% H_2 or O_2.

Another method to differentiate between Schottky-barrier and Poole–Frenkel conduction is to examine the leakage behavior when the top and bottom electrodes are composed of materials with different work functions.[41] Ag ($\Phi_B = 3.6$ eV), Au ($\Phi_B = 5.1$ eV), and Pt ($\Phi_B = 5.4$ eV) electrodes were deposited on the surface of $BaTiO_3$ films and leakage was measured as a function of the top electrode material and the polarity of the applied voltage. The value of leakage current density for the different electrode arrangements was measured under an applied field of 300 kV/cm, where conduction was limited by thermionic emission of electrons. The results of this experiment are summarized in Table 4. The leakage current strongly depended on the injection electrode material. For example, when both electrodes were Pt (the Pt/Pt electrode configuration), the leakage current was $1.64 \cdot 10^{-3}$ A/cm^2. When the injection electrode was changed to either Au or Ag (Au/Pt or Ag/Pt

Table 3
Barrier height and trap depth values for $BaTiO_3$ thin films

	Barrier height (eV)	Trap depth (eV)
As-formed (anneal 150 °C)	0.45	0.53
Ar–5% H_2 (anneal 500 °C)	0.63	0.72
O_2 (anneal 500 °C)	0.64	0.72

Table 4
Leakage current for $BaTiO_3$ thin film capacitors under a 300 kV/cm applied electric field

Electrode configuration	Injection electrode	Leakage (A/cm^2)
Pt/Pt	Pt	$1.64 \cdot 10^{-3}$
Pt/Au	Pt	$1.73 \cdot 10^{-3}$
Pt/Ag	Pt	$1.80 \cdot 10^{-3}$
Au/Pt	Au	$15.5 \cdot 10^{-3}$
Ag/Pt	Ag	$146 \cdot 10^{-3}$

configurations), the leakage increased to $15.5 \cdot 10^{-3}$ A/cm^2 and $146 \cdot 10^{-3}$ A/cm^2 respectively. In each case, reversing the voltage polarity (to make Pt the injection electrode) resulted in values similar to the Pt/Pt configuration.

Based on the experimental results discussed above, the leakage current of the hydrothermal $BaTiO_3$ films in this study depended on two factors. First, conductivity decreased by over an order of magnitude following annealing in either oxidizing or reducing atmospheres, and in each case the barrier height increased. This suggests that annealing reduces the overall defect concentration and/or interface state density, and some portion of the leakage current may be due to a Poole–Frenkel-type mechanism. Second, leakage depended on the electrode material and therefore the electrode work function. This indicates that leakage is controlled at least partially by Schottky-barrier-limited conduction. Thus, it appears likely that conduction is dependent on some combination of Poole–Frenkel and Schottky-barrier controlled processes.

4. Summary

- TiO_2 films processed at 90 °C in 1.0M $Ba(OH)_2$ reacted to form $BaTiO_3$ in as little as 1 h. Films grown on (100) $SrTiO_3$ suggested that $BaTiO_3$ nucleation occurred at the film-substrate interface as well as the film-solution interface.
- Annealing in air caused the lattice parameter to contract beginning at temperatures below 200 °C.
- Annealing $BaTiO_3$ films in air at temperatures ranging from 200 to 500 °C resulted in decreases in the dielectric constant, tanδ, and leakage current, and an increase in the zero-field barrier height.
- Annealing reduced the dependence of the dielectric constant on the frequency of the applied field.
- The mechanism of electronic conduction in the thin films occurred by a combination of Poole–Frenkel and Schottky-barrier controlled processes.

Acknowledgements

The authors wish to acknowledge the National Science Foundation for its support of this research, under grant DMR-9623744. The authors also wish to acknowledge the contributions of Adam Chamberlain during his summer 2001 visit to Purdue University through the REU program (DMR-9912195).

References

1. Scott, J. F., High-dielectric constant thin films for dynamic random access memories (DRAM). *Ann. Rev. Mater. Sci.*, 1998, **28**, 79–100.
2. Tahan, D. M., Safari, A. and Klein, L. C., Preparation and characterization of $Ba_xSr_{1-x}TiO_3$ thin films by a sol-gel technique. *J. Am. Ceram. Soc.*, 1996, **79**(6), 1593–1598.
3. Hennings, D., Barium titanate based ceramic materials for dielectric use. *Int. J. High Technol. Ceram.*, 1987, **3**, 91–111.
4. Vendik, O. G., Hollmann, E. K., Kozyrev, A. B. and Prudan, A. M., Ferroelectric tuning of planar and bulk microwave devices. *J. Superconductivity*, 1999, **12**(2), 325–338.
5. Kotecki, D. E., Baniecki, J., Shen, H., Laibowitz, R., Saenger, K., Lian, J., Shaw, T., Athavale, S., Cabral, C., Duncombe, P., Gutsche, M., Kunkel, G., Park, Y., Wang, Y. and Wise, R., (Ba,Sr)TiO_3 dielectrics for future stacked-capacitor DRAM. *IBM J. Res. Develop.*, 1999, **43**(3), 367–380.
6. Yoshimura, T., Fujimura, N. and Ito, T., The initial stage of $BaTiO_3$ epitaxial films on etched and annealed $SrTiO_3$ substrates. *J. Cryst. Growth*, 1997, **174**, 790–795.
7. Xu, J. J., Shaikh, A. S. and Vest, R. W., High K $BaTiO_3$ films from metalloorganic precursors. *IEEE Trans. Ultrason. Ferroelec. Freq. Contr.*, 1989, **36**(3), 307–311.
8. Sharma, H. B. and Mansingh, A., Phase transition in sol-gel-derived barium titanate thin films. *J. Phys. D—Appl. Phys.*, 1998, **31**(13), 1527–1533.
9. Kullmer, R., Dielectric and ferroelectric properties of pulsed-laser deposited $BaTiO_3$ films. *Appl. Phys. A*, 1997, **65**, 273–279.
10. Chen, S.-Y. and Chen, I.-W., Cracking during pyrolysis of oxide thin filmsphenomenology, mechanisms, and mechanics. *J. Am. Ceram. Soc.*, 1995, **78**(11), 2929–2939.
11. Kwok, C. K. and Desu, S. B., Low temperature perovskite formation of lead zirconate titanate thin films by a seeding process. *J. Mater. Res.*, 1993, **8**(2), 339–344.
12. Lencka, M. M. and Riman, R. E., Thermodynamic modeling of hydrothermal synthesis of ceramic powders. *Chem. Mater.*, 1993, **5**, 61–70.
13. Dawson, W. J., Hydrothermal synthesis of advanced ceramic powders. *Ceram. Bull.*, 1988, **67**(10), 1673–1678.
14. Xu, J. J., Shaikh, A. S. and Vest, R. W., High K $BaTiO_3$ films from metalloorganic precursors. *IEEE Trans. Ultrason. Ferroelec. Freq. Contr.*, 1989, **36**(3), 307–311.
15. Shaikh, A. S. and Vest, G. M., Kinetics of $BaTiO_3$ and $PbTiO_3$ formation from metallo-organic precursors. *J. Am. Ceram. Soc.*, 1986, **69**(9), 682–688.
16. Slamovich, E. B. and Aksay, I. A., Hydrothermal processing of polymer/$BaTiO_3$ films. In *MRS Symp. Proc. v. 346, Better Ceramics through Chemistry VI*, ed. A. K. Cheetham, C. J. Brinker, M. L. Mecartney and C. Sanchez. Materials Research Society, Warrendale, PA, 1994, pp. 63–68.
17. Roeder, R. K. and Slamovich, E. B., Assessment of the critical thickness and fracture toughness of thin metal-organic precursor films. *Ceramic Transactions*, 1998, **83**, 375–382.
18. Dietz, G.W., Antpöhler, W., Klee, M. and Waser, R., Electrode influence on the charge transport through $SrTiO_3$ thin films. *J. Appl. Phys.*, 1995, **78**(10), 6113–6121.
19. McCormick, M. A. and Slamovich, E. B., Effect of precursor pyrolysis on the dielectric properties of hydrothermally derived $BaTiO_3$ thin films. *J. Am. Ceram. Soc.*, 2000, **82**(2), 442–444.
20. Software Manual for Siemens DIFFRAC-AT v.3.1 and Profile Fitting Program v.1.5. Siemens Analytical X-Ray Instruments, Cherry Hill, NJ, 1988.
21. Dietz, G. W., Schumacher, M., Waser, R., Strieffer, S. K., Basceri, C. and Kingon, A. I., Leakage currents in $Ba_{0.7}Sr_{0.3}TiO_3$ thin films for ultrahigh-density dynamic random access memories. *J. Appl. Phys.*, 1997, **82**(5), 2359–2364.
22. JCPDS Card Number 31-174.

23. Kingery, W. D., Bowen, H. K. and Uhlmann, D. R., *Introduction to Ceramics*. John Wiley & Sons, New York, 1960 pp. 947–951.
24. Slamovich, E. B. and Aksay, I. A., Structure evolution in hydrothermally processed (<100 °C) $BaTiO_3$ films. *J. Am. Ceram. Soc.*, 1996, **79**(1), 239–247.
25. Shi, E., Xia, C., Zhong, W., Wang, B. and Feng, C., Crystallographic properties of hydrothermal barium titanate crystallites. *J. Am. Ceram. Soc.*, 1997, **80**(6), 1567–1572.
26. Busca, G., Buscaglia, V., Leoni, M. and Nanni, P., Solid-state and surface spectroscopic characterization of $BaTiO_3$ fine powders. *Chem. Mater.*, 1994, **6**, 955–961.
27. JCPDS Card Number 31-174.
28. Wada, S., Suzuki, T. and Noma, T., Role of lattice defects in the size effect of barium titanate fine particles. *J. Ceram. Soc. Japan*, 1996, **104**(5), 383–392.
29. Chien, A. T., Xu, X., Kim, J. H., Sachleben, J., Speck, J. S. and Lange, F. F., Electrical characterization of $BaTiO_3$ heteroepitaxial thin films by hydrothermal synthesis. *J. Mater. Res.*, 1999, **14**(8), 3330–3339.
30. Wada, S., Suzuki, T. and Noma, T., Preparation of barium titanate fine particles by hydrothermal method and their characterization. *J. Ceram. Soc. Japan*, 1995, **103**, 1220–1227.
31. Takeuchi, T., Tabuchi, M., Ado, K., Honjo, K., Nakamura, O., Kageyama, H., Suyama, Y., Ohtori, N. and Nagasawa, M., Grain size dependence of dielectric properties of ultrafine $BaTiO_3$ prepared by a sol-crystal method. *J. Mater. Sci.*, 1997, **32**, 4053–4060.
32. McCormick, M. A., Roeder, R. K. and Slamovich, E. B., Processing effects on the composition and dielectric properties of hydrothermally derived $Ba_xSr_{(1-x)}TiO_3$ thin films. *J. Mat. Res.*, 2001, **16**(4), 1200–1209.
33. O'Dwyer, J. J., *The Theory of Electrical Conduction and Breakdown in Solid Dielectrics*. Clarendon Press, Oxford, UK, 1973.
34. Kao, K. C. and Hwang, W., *Electrical Transport in Solids*. Pergamon, New York, 1981.
35. Formenko, V. S. In *Handbook of Thermionic Properties*, ed. G. V. Samsonov. Plenum Press Data Division, New York, 1966.
36. Hafid, L., Godefroy, G., El Idrissi, A. and Michel-Calendini, F., Absorption spectrum in the near U. V. and electronic structure of pure barium titanate. *Solid State Commun.*, 1988, **66**(8), 841–845.
37. Begg, B. D., Vance, E. R. and Nowotny, J., Effect of particle size on the room-temperature crystal structure of barium titanate. *J. Am. Ceram. Soc.*, 1994, **77**(12), 3186–3192.
38. Jonscher, A. K. and Hill, R. M., In *Physics of Thin Films*, Vol. 8, ed. Georg Hass. Academic, New York, 1975. p. 222.
39. Sze, S. M., *Physics of Semiconductor Devices*. John Wiley & Sons, New York, 1969.
40. Dietz, G. W. and Waser, R., Charge injection in $SrTiO_3$ thin films. *Thin Solid Films*, 1997, **299**, 53–58.
41. Al-Shareef, H. N. and Dimos, D., Leakage reliability characteristics of lead zirconate titanate thin-film capacitors. *J. Am. Ceram. Soc.*, 1997, **80**(12), 3127–3132.